small NANO MICRO

Self-Supported PtAuP Alloy Nanotube Arrays with Enhanced Activity and Stability for Methanol Electro-Oxidation

Lili Zhang, Liang-Xin Ding, Hongbin Chen, Dongdong Li, Suqing Wang, and Haihui Wang**

Inhibiting CO formation can more directly address the problem of CO poisoning during methanol electro-oxidation. In this study, 1D self-supported porous PtAuP alloy nanotube arrays (ANTAs) are synthesized via a facile electro-codeposition approach and present enhanced activity and improved resistance to CO poisoning through inhibiting CO formation (non-CO pathway) during the methanol oxidation reaction in acidic medium. This well-controlled Pt-/transition metal-/nonmetal ternary nanostructure exhibits a specific electroactivity twice as great as that of PtAu alloy nanotube arrays and Pt/C. At the same time, PtAuP ANTAs show a higher ratio of forward peak current density (I_f) to backward peak current density (I_b) (2.34) than PtAu ANTAs (1.27) and Pt/C (0.78). The prominent I_f/I_b value of PtAuP ANTAs indicates that most of the intermediate species are electro-oxidized to carbon dioxide in the forward scan, which highlights the high electroactivity for methanol electro-oxidation.

Considerable research has been devoted to the commercialization of direct methanol fuel cells (DMFCs) as a promising alternative power source in terms of high energy density, convenient handling, and environmental friendliness.[1] Platinum (Pt) and Pt group metals are thought to be the best electrocatalysts[2] for the oxidation of methanol. However, two major disadvantages, (i) prohibitive cost and limited reserves of Pt[3] and (ii) poor durability because of low tolerance to CO-like poisoning species,[4] have hindered the large-scale development of pure Pt in DMFCs. Accordingly, efforts have been focused on engineering the morphology and composition of Pt-based catalysts to overcome the above obstacles.[5] So far, substantial research has shown that PtM (M: non-platinum metal) bimetallic catalysts with a well-defined 1D shape have enhanced activity and improved resistance to poisoning, while minimizing platinum content for the methanol oxidation reaction (MOR), influenced by modifications in the structural and electronic effects between different elements.[3a,6]

Among the non-platinum materials, Au nanoparticles and Au nanoclusters have been shown to have prominent CO oxidation behavior.[7] Additionally, Au has not only perfect stability in acidic conditions[8] but also particular effects on Pt, since it is more electronegative than Pt.[9] Therefore, platinum–gold (Pt–Au) nanostructures have received special attention as DMFCs electrocatalysts due to their unique electronic and electrocatalytic properties.[10] In recent years, various types of Pt–Au nanostructures have been synthesized, such as core–shell Au–Pt nanoparticles,[11] dendritic Au–Pt,[7a] PtAu nanotubes,[12] Pt–Au nanoparticles,[13] and Pt–Au hollow nanourchins.[6b] However, Pt–Au catalysts are still expensive. To reduce costs and further improve the catalytic performance, incorporating a third cheaper metal into the PtAu system is a current widely used strategy.[14] For example, Sun et al. reported that core/shell Au/CuPt nanoparticles

L. Zhang, Prof. L.-X. Ding, H. Chen, D. Li,
Dr. S. Wang, Prof. H. Wang
School of Chemistry and Chemical Engineering
South China University of Technology
No. 381 Wushan Road, Guangzhou 510640, China
E-mail: lxding@scut.edu.cn; hhwang@scut.edu.cn

DOI: 10.1002/smll.201604000

have higher activity and durability than commercial 5 nm Pt and a negligible loss of 7.8% of their electrochemically active surface areas (ECSAs) after 5000 cycles.[14a] Dutta and Ouyang fabricated NiAuPt nanoparticles on reduced graphene oxide ($Ni_{40}Au_{33}Pt_{27}$-NGs) as an electrocatalyst for MOR, which displayed 36% higher current density than that of $Au_{55}Pt_{45}$-NGs.[14e] Although these efforts significantly reduced the amount of Pt used and improved their electrocatalytic activity toward the methanol oxidation reaction, their durability is still not satisfactory due to the possibility of Ostwald ripening and gradually accumulated CO-like poisoning species during the electrocatalytic process. In other words, the development of efficient fuel cell electrocatalysts with high activity and durability is still a great challenge.

It is well-known that the complete electro-oxidation of methanol to CO_2 on Pt or Pt-based catalysts proceeds through CO or non-CO pathways in acidic medium.[15] In general, the mitigation of CO poisoning of Pt-based nanocatalysts by incorporating Au or other active metals has been attributed to the facile removal of CO and CO-like species adsorbed on the Pt surface, which resulted from electronic effects and a bifunctional mechanism.[16] For the former, the modified surface of the Pt atom has weaker CO adsorption energy, while in the latter, hydroxyl groups adsorbed by the non-platinum metal work to oxidize CO at lower potential than pure Pt.[17] For comparison, some researchers have put forward a non-CO-involving pathway, that is, inhibiting CO formation rather than facilitating CO removal results in enhanced CO poisoning resistance, which might be a more direct pathway to address the problem of CO poisoning during methanol electro-oxidation.[4a,15c,17,18] Obviously, in this regard, it is highly desirable to develop novel catalysts with increased ability for CO oxidation or resistance of CO formation (non-CO pathway) to improve the activity and durability toward methanol oxidation.

Recent advances have revealed that dilution of the active metal by nonmetal elements can provide better opportunities for enhancing the electrocatalytic activity and durability in small organic molecule oxidation.[19] A typical nonmetallic element is phosphorus (P). It has abundant valence electrons, similar to nitrogen, which can effectively modify the electronic state of the active metal and thus tailor the physical-chemical properties. For example, Xing and co-workers doped P in Pt-Ru/C to form Pt-Ru-P/C, which not only increased the electrochemically active surface area of the catalyst but also led to high activity and enhanced resistance to CO poisoning compared with Pt-Ru/C.[19g] Thus, P doping into Pt–Au catalysts should be a promising approach for further increasing the electrocatalytic activity and CO tolerance.

Combining the above considerations, we present here the facile synthesis of porous PtAuP alloy nanotube arrays (ANTAs) and demonstrate their enhanced activity and stability for MOR in acidic medium. PtAuP ANTAs were easily prepared by galvanostatic electrodeposition using ZnO nanorod arrays (NRAs) as templates, as illustrated in **Scheme 1**. Notably, this high-performance electrocatalyst, with a 1D bimetal and nonmetal co-doping alloy nanotube architecture, has the following merits: (i) the support-less, interconnected, porous nanotube arrays composed of interconnected nanoparticles not only combines the advantages of 1D and 0D structures but more importantly, promotes the transfer of active species and improves the utilization of platinum; (ii) compared with transition metals, the nonmetallic element phosphorus added to the PtAuP alloy structure can avoid anodic dissolution and leaching of the base metals in acidic medium; (iii) the alloy-type structure that formed from

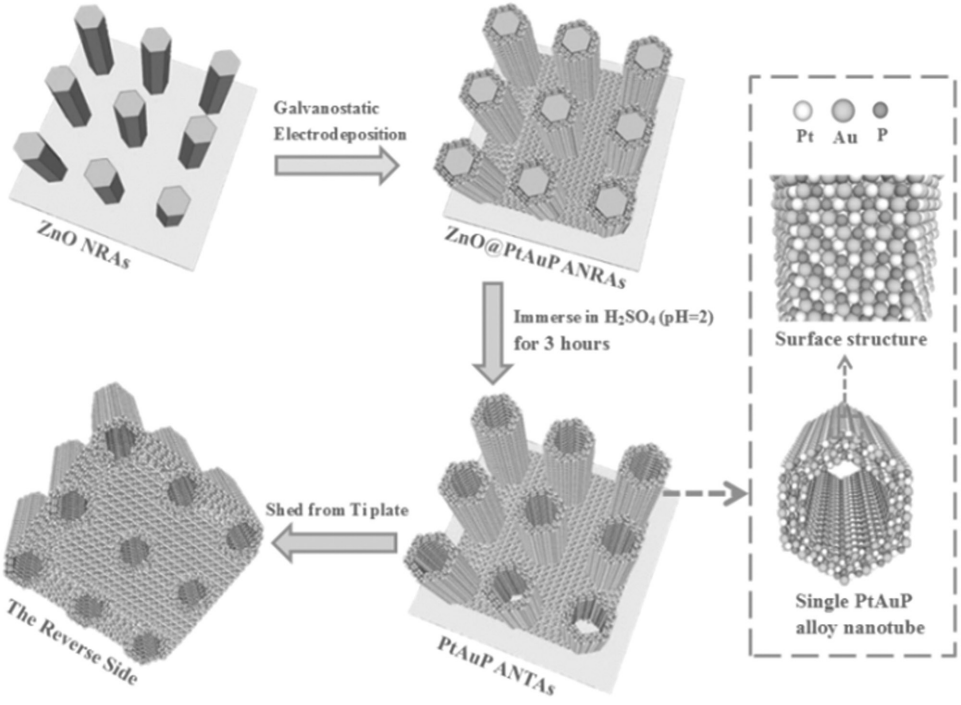

Scheme 1. Schematic illustration for the synthesis of PtAuP alloy nanotube arrays.

the atomic-level mixture can enhance the mutual influence among the three elements Pt, Au, and P; and (iv) this Pt-/transition metal-/nonmetal ternary alloy catalyst can provide the more straightforward strategy of inhibiting CO formation to address CO poisoning during the complete electrooxidation of methanol. Benefiting from the integration of the composition and architecture, such self-supported porous PtAuP ANTAs catalyst shows enhanced MOR activity, excellent long-term durability, and high anti-poisoning ability by inhibiting CO formation in acidic medium.

The scanning electron microscopy (SEM) images in **Figure 1**a show that the synthesized ZnO NRAs are vertical to the Ti substrate, and these highly ordered ZnO nanorods are ≈1.5 µm in length with diameters of 250–300 nm (inset in Figure 1a). The SEM and transmission electron microscopy (TEM) images of the ZnO@PtAuP core–shell nanorod arrays are shown in Figure S1 and Figure S2 in the Supporting Information, respectively, demonstrating that the PtAuP nanoparticles uniformly coat the ZnO nanorods. Figure 1b provides typical SEM images of PtAuP ANTAs. It is clear that these PtAuP alloy nanotubes are uniform and link together to form a sheet. In addition, the bottom view of the overturned sample in the lower right triangle area of Figure 1b presents a honeycomb-like morphology, indicating that a hollow nanotube array structure of PtAuP alloy formed successfully using ZnO NRAs as templates. More meaningfully, the PtAuP alloy nanotubes are interconnected at the bottom, which promotes the transfer of active species between nanotube arrays. The magnified SEM image shown in the inset of Figure 1b further confirms the hollow structure of the PtAuP alloy nanotubes.

The morphology and structure of PtAuP ANTAs were further investigated by TEM. Figure 1c shows a typical TEM image of the PtAuP alloy nanotube, and the inner diameter is consistent with the SEM images discussed above. More remarkably, Figure 1c reveals that the nanotube wall has a nanoporous structure, and the wall thickness is ≈25 nm. In addition, the PtAuP ANTAs are polycrystalline, as evidenced by the multiple diffraction rings in the selected area electron diffraction (SAED) pattern in the inset of Figure 1c. The magnified TEM image shown in Figure 1d further confirms that the PtAuP alloy nanotube wall is porous and moreover, consists of the interconnected homogeneous nanocrystals with a size of ≈4–5 nm. The detailed structure of a single PtAuP nanoparticle was studied by high-resolution TEM, as shown in Figure S3 in the Supporting Information. Lattice fringes can be observed with interplanar spacings of 0.230 and 0.200 nm, assigned to the (111) and (200) facets of the PtAuP alloy, respectively. It is worth noting that the interplanar lattice distance of the PtAuP alloy is between that of pure Pt and Au; taking the (111) facet as an example, its lattice distance in the PtAuP alloy (0.230 nm) is slightly larger than that of pure Pt (0.227 nm) but smaller than that of pure Au (0.235 nm). Such phenomenon indicates the formation of the alloy structure.

The structural composition of the as-synthesized catalysts was further confirmed by X-ray diffraction (XRD). The XRD results in Figure S4 in the Supporting Information demonstrate that all of the parallel-synthesized PtAuP ANTAs, PtAu ANTAs, Pt NTAs, and Au NTAs have a face-centered-cubic (fcc) structure. The (111) peaks for Pt NTAs and Au NTAs were located at 39.76 and 38.20, respectively, which agrees with the original peak positions of their fcc metallic states. After mixing Pt NTAs and Au NTAs, we found two (111) peaks that correspond to separated Pt and Au phases. Interestingly enough, no additional (111) peak was observed in the tested PtAuP ANTAs and PtAu ANTAs, and the (111) peaks of PtAuP ANTAs and PtAu ANTAs were shifted to lower angles compared to Pt NTAs but shifted to higher angles compared to Au NTAs. The single set of fcc diffraction peaks and such peak shifts confirm the good formation of the alloy structure. In addition, the XRD patterns of PtAu ANTAs and PtAuP ANTAs obtained over a narrowed scope at a decreased sweep rate (Figure S5, Supporting Information) indicate that there is a weak shift in the (111) peak between PtAu ANTAs and PtAuP ANTAs, which results from the weak alloying degree of PtAuP ANTAs due to the low content of phosphorus. PtAuP ANTAs were further

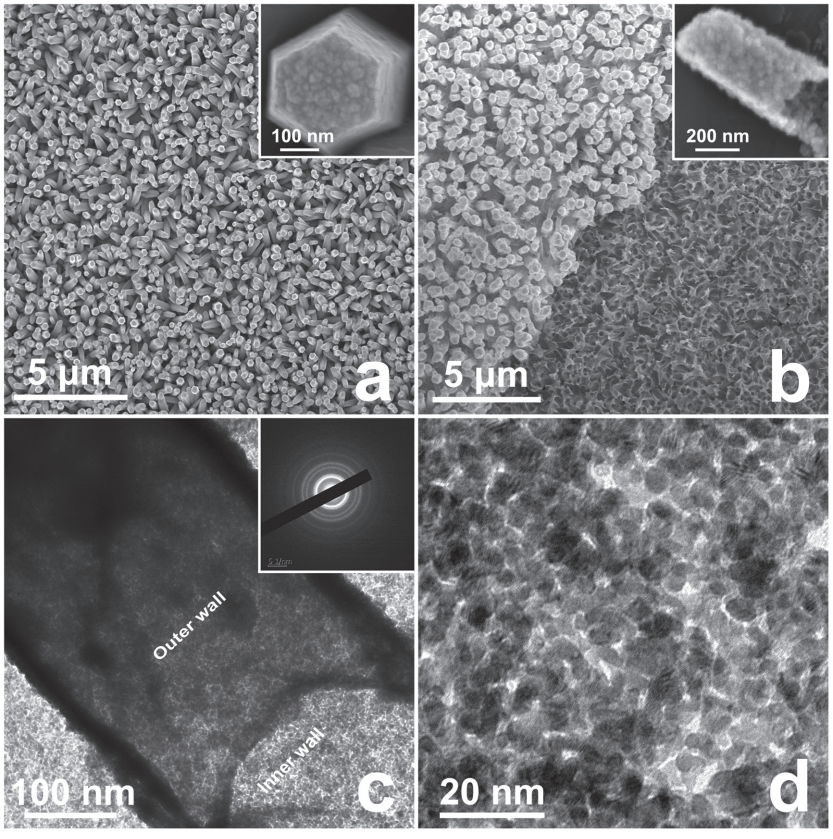

Figure 1. SEM images of a) ZnO nanorod arrays and b) PtAuP ANTAs. The insets in (a) and (b) are the high magnification SEM images. c,d) TEM images and SAED pattern (inset in (c)) of PtAuP ANTAs.

analyzed by energy dispersive X-ray spectroscopy (EDS). As shown in Figure S6 in the Supporting Information, the strong spectral peaks of Pt, Au, and P suggest the successful codeposition of these three elements. Quantitative analysis from EDS shows 41.77 at% Pt, 51.61 at% Au, and 6.62 at% P in the PtAuP nanotubes. The elemental distribution in the PtAuP alloy nanotubes was examined by EDS mapping. Figure S7 in the Supporting Information shows that the three elements Pt, Au, and P are homogeneously distributed in the PtAuP nanotube wall, illustrating a homogeneous PtAuP alloy distribution, which provides a high-quality PtAuP alloy nanotube.

To further investigate the surface composition and the valence state, X-ray photoelectron spectroscopy (XPS) measurements were carried out on PtAuP ANTAs and PtAu ANTAs, and the results are shown in **Figure 2**a–d. Figure 2a,b shows the Pt 4f and Au 4f regions of the above catalysts. Compared to those of PtAu ANTAs, the Pt 4f and Au 4f peaks of PtAuP ANTAs were both shifted to lower binding energies (≈0.11 and 0.05 eV, respectively), which indicates that there are strong interaction between Pt, Au, and P. The P 2p region in the XPS spectra (Figure 2c,d) shows that the element P exists in PtAuP ANTAs. In addition, the peak at 133.08 eV (Figure 2c) is assigned to oxidized P arising from the superficial oxidation of PtAuP ANTAs.

The electrocatalytic performance of the as-prepared porous PtAuP ANTAs was evaluated, along with that of the porous PtAu ANTAs and commercial Pt/C (20% Pt, Johnson Matthey) for comparison. **Figure 3**a shows the cyclic voltammetry (CV) curves of these three catalysts, which are recorded in N_2-purged 0.5 M H_2SO_4 solution at a scan rate of 50 mV s^{-1}. The ECSAs of these catalysts can be estimated from the areas of the hydrogen adsorption/desorption region after double-layer correction, exhibited in the distinct potential region between 0.0 and 0.35 V. According to the equation given in previous studies,[20] the calculated ECSA of PtAuP ANTAs is 21.8 m^2 g^{-1}_{Pt}, which is larger than that for PtAu ANTAs of 14.5 m^2 g^{-1}_{Pt}. The enhanced ECSA of PtAuP ANTAs may be the result of the more uniform dispersion of PtAuP alloy nanoparticles resulting from the effect of P on the electronic state of Pt and Au. Though the interconnected nanoparticle structure and alloy form can occupy a large portion of the active metal interface, leading to the ECSA of PtAuP ANTAs being less than 50% of that of commercial Pt/C (57.9 m^2 g^{-1}_{Pt}), the specific activity of the catalyst is improved.

The electrocatalytic activities of PtAuP ANTAs, PtAu ANTAs, and commercial Pt/C toward MOR were investigated in 0.5 M CH_3OH + 0.5 M H_2SO_4 solution at 50 mV s^{-1}. The resulting CV curves (Figure 3b) exhibit that the peak current density of PtAuP ANTAs in the forward scan is obviously higher than that of PtAu ANTAs (≈2.13 times) and commercial Pt/C (≈2.72 times), implying that PtAuP ANTAs have improved specific electroactivity for MOR. It is well known that the backward scan corresponds to the electro-oxidation of the residual carbonaceous species generated during the forward scan.[21] Therefore, a high ratio of forward peak current density to backward peak current density (I_f/I_b) implies the efficient, complete electro-oxidation of methanol and less accumulation of intermediate species on the electrocatalyst.[22] From Figure 3b, the I_f/I_b ratio of PtAuP ANTAs, PtAu ANTAs, and commercial Pt/C are 2.34, 1.27, and 0.78, respectively. The prominent I_f/I_b value of PtAuP

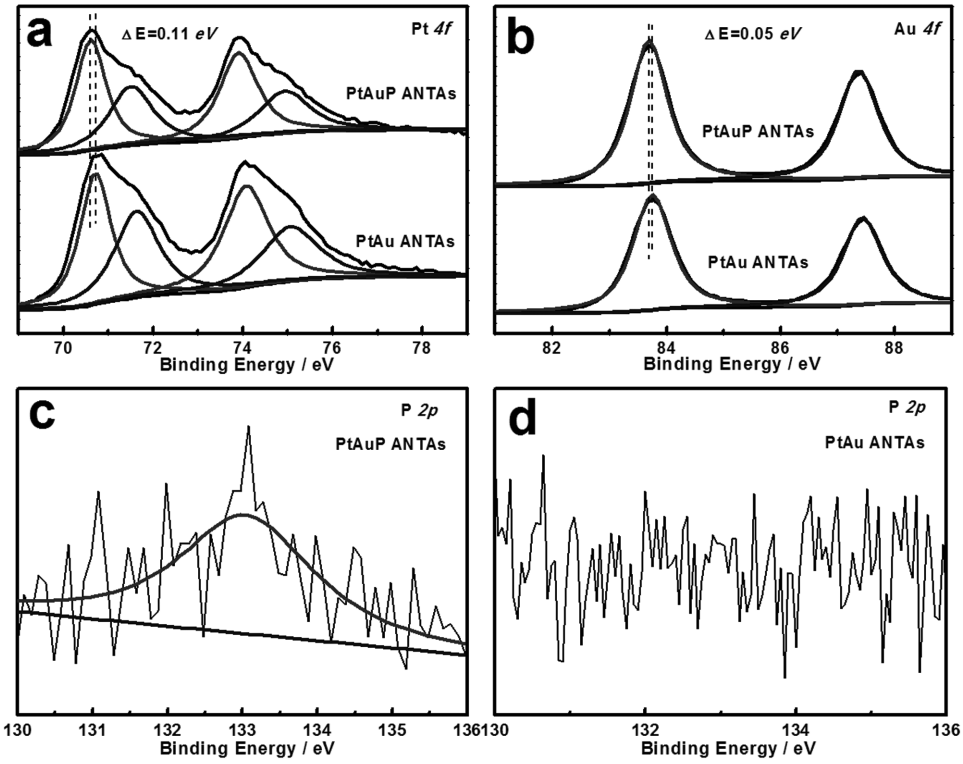

Figure 2. XPS spectra of a) Pt 4f, b) Au 4f for PtAuP ANTAs, and PtAu ANTAs. XPS spectral of P 2p for c) PtAuP ANTAs and d) PtAu ANTAs.

ANTAs indicates that most of the intermediate species were electro-oxidized to carbon dioxide in the forward scan, which highlights the high electroactivity for MOR. Figure S8 in the Supporting Information shows two CV curves for AuP NTAs obtained in 0.5 M H_2SO_4 and 0.5 M CH_3OH + 0.5 M H_2SO_4, respectively; the two similar curves indicate that AuP NTAs have almost no electrocatalytic activity for MOR in acidic medium. Meanwhile, the result of CO stripping measurements on PtP NTAs and PtAuP ANTAs electrodes (Figure S9, Supporting Information) shows that the CO stripping potential on PtP NTAs was obviously lower than that on PtAuP ANTAs. These results indicated that, influenced by Au atom, the surface of the Pt atom in PtAuP ANTAs became electron rich and donated more electrons to CO 2Π* orbitals, thus strengthening CO adsorption.[23] Thus, the enhanced electroactivity of PtAuP ANTAs does not follow a bifunctional mechanism but the addition of Au modifies the surface of the Pt atom.[4a] In addition, note that the scission of C−H and O−H bonds is critical for methanol electro-oxidation.[15b] By combining the XPS results, we are convinced that the much higher specific activity of PtAuP ANTAs compared to PtAu ANTAs can be attributed to the incorporation of P, resulting in a lower barrier for the dehydrogenation reaction due to the increased electron density on the Pt atoms.

It is widely agreed that the ratio of I_f/I_b can also be used to describe the resistance to CO poisoning, and reduced CO poisoning results from either the facile removal of CO species chemisorbed on the Pt surface or the resistance to CO formation. To confirm the electrocatalytic properties of the above electrocatalysts toward CO oxidation, CO-stripping measurements were performed in a solution of 0.5 M H_2SO_4. The higher CO oxidation potential of PtAu ANTAs (Figure 3c) and PtAuP ANTAs (Figure 3d) compared with commercial Pt/C (Figure S10, Supporting Information) indicates that PtAu ANTAs and PtAuP ANTAs more strongly absorb CO than commercial Pt/C, that is, the decreased CO poisoning on PtAu ANTAs and PtAuP ANTAs should be ascribed to the restricted CO formation rather than the facile removal of CO from the active sites. This phenomenon agrees with that for PtAu(111) reported in the literature.[13b,17,18] According to the mechanism of methanol electro-oxidation,[18] the disparity between the CO pathway ($CH_3OH \rightarrow CH_2O \rightarrow CHO \rightarrow CO + OH_{ads} \rightarrow CO_2$) and non-CO pathway ($CH_3OH \rightarrow CH_2O \rightarrow CHO + OH_{ads} \rightarrow HCOOH \rightarrow CO_2$) begins after CH_2O forms, and the priority for the OH_{ads} reaction or dehydrogenation decides the reaction route of methanol electro-oxidation. In addition, the XPS analysis and CO stripping measurements indicated that the electronic structure and density of states of the active metal (Pt) are changed by interactions among Pt, Au, and P. Thus, we believe that the electronic effect not only reduces the activation energy of methanol but also strengthens the activation of water molecules,[24] which promote the reaction of CHO with OH_{ads} and then the non-CO pathway proceeds. More interestingly, unlike the CO-stripping curves of PtAu ANTAs, a non-CO oxidation peak was observed in the first forward scan on PtAuP ANTAs catalyst. However, chemisorbed CO could be removed from the surface along with the oxidation of Pt, judging by the subsequent appearance of the hydrogen adsorption/desorption region and the weaker

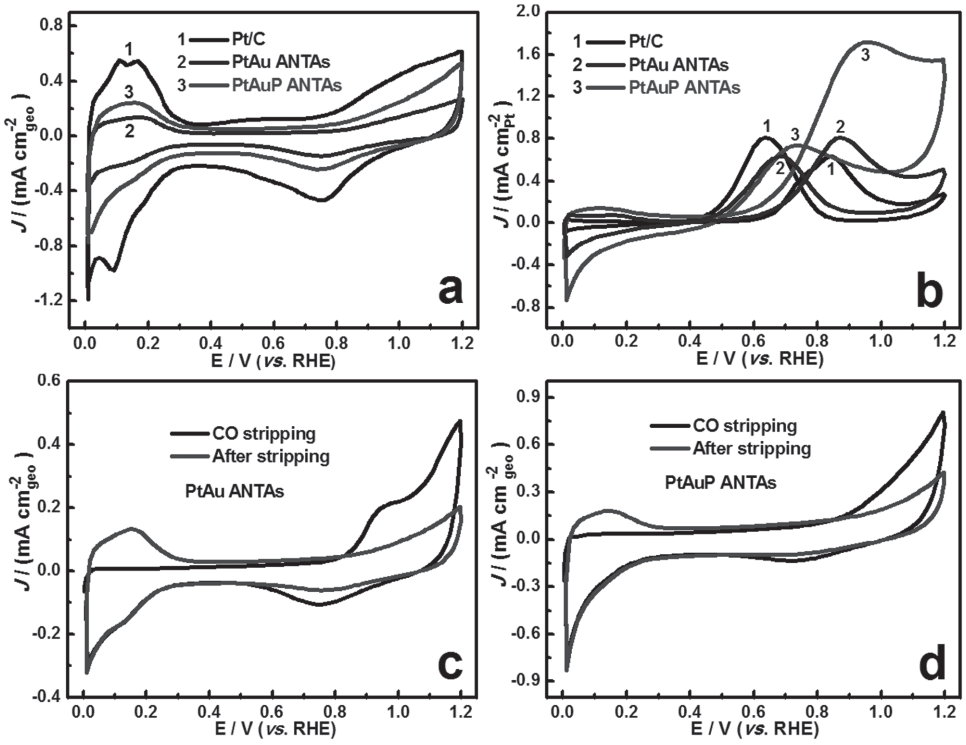

Figure 3. a) CVs for PtAuP ANTAs, PtAu ANTAs, and Pt/C in N_2-purged 0.5 M H_2SO_4 at a scan rate of 50 mV s^{-1}. b) CVs for PtAuP ANTAs, PtAu ANTAs, and Pt/C in 0.5 M CH_3OH + 0.5 M H_2SO_4 at 50 mV s^{-1}. CO stripping voltammograms on c) PtAu ANTAs and d) PtAuP ANTAs performed in 0.5 M H_2SO_4 solution at 50 mv s^{-1}. (Pt loading: ≈14 μg cm^{-2}, S = 0.07065 cm^2_{geo}).

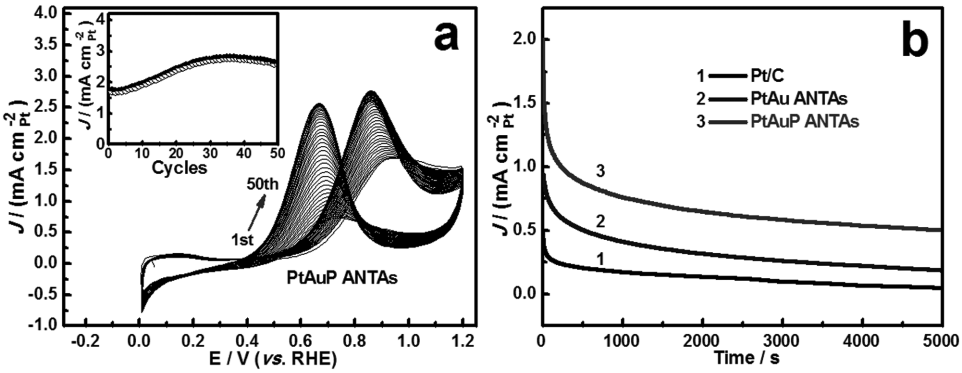

Figure 4. a) CVs of PtAuP ANTAs from the 1st to 50th cycle in 0.5 M CH_3OH + 0.5 M H_2SO_4 at 50 mV s^{-1} (inset: change in the peak current density in the forward scan). b) Chronoamperometry curves for PtAuP ANTAs, PtAu ANTAs and Pt/C held at 0.84 V (vs RHE) in 0.5 M CH_3OH + 0.5 M H_2SO_4 mixed solution at 50 mV s^{-1}. (Pt loading: ≈14 μg cm^{-2}, S = 0.07065 cm^2_{geo}).

oxidation peak of Pt in the second forward scan. These observations implied that the adsorption between CO and the active sites on the PtAuP ANTAs surface was stronger than that for PtAu ANTAs because of the lower binding energy of Pt $4f_{7/2}$. A deeper insight is that PtAuP ANTAs are better at preventing CO formation to eliminate CO poisoning compared with PtAu ANTAs.

Figure 4a shows the continuous CV curves of PtAuP ANTAs, where the inset corresponds to the change in peak current density in the forward scan with increasing cycle number. It is clearly seen that the electrocatalytic activity of PtAuP ANTAs has a gradual increasing trend, as well as increasingly high peak current density and more negative peak potential in the forward scan, which can result from the activation of the active sites. After activation, the improved specific activity of PtAuP ANTAs compared to PtAu ANTAs (Figure S11, Supporting Information) and commercial Pt/C (Figure S12, Supporting Information) is much higher than the initial value.

To further evaluate the anti-poisoning capacity of these catalysts, the durability in MOR was characterized by chronoamperometry curves, as shown in Figure 4b. It can be seen that PtAuP ANTAs catalyst shows a slower decay in activity than PtAu ANTAs and commercial Pt/C. This long-term performance of PtAuP ANTAs indicates its excellent properties toward anti-poisoning. In addition, initial rapid current decay for all catalysts was observed, possibly due to double-layer discharge, hydrogen adsorption, and intermediate species, such as CH_2O and CHO, occupying the active sites during the oxidation reaction, as previously reported.[25] However, even after a 5000 s stability test, the specific activity of PtAuP ANTAs catalyst is still higher than that of PtAu ANTAs and commercial Pt/C, confirming the greater electroactivity and stability of PtAuP ANTAs catalyst for methanol oxidation.

In summary, a well-designed Pt-/transition metal-/nonmetal ternary alloy catalyst with a porous nanotube structure, PtAuP ANTAs, was facilely synthesized for use as an electrocatalyst for methanol oxidation. PtAuP ANTAs show enhanced electroactivity and high anti-poisoning ability though a non-CO pathway in acidic medium. Specifically, this work proves that the addition of P can lead to the homogeneous distribution of nanocrystals and an increased ECSA of PtAuP alloy nanotubes compared to PtAu nanotubes. Moreover, PtAuP (111) more strongly absorbs CO than PtAu(111) but presents the more powerful ability of inhibiting CO formation to avoid CO poisoning during methanol electrooxidation.

Experimental Section

Materials Synthesis: All galvanostatic electrodeposition were achieved in a two-electrode electrolytic cell and the graphite electrode was used as a counter electrode (spectral grade, 1.8 cm^2). The synthesis of porous PtAuP alloy nanotube arrays is described in the following procedures. ZnO nanorod arrays (NRAs) template was firstly prepared by galvanostatic electrolysis in mixed solution of 0.01 M $Zn(NO_3)_2$ + 0.05 M NH_4NO_3 at 0.5 mA cm^{-2} for 90 min at 70 °C on Ti plates (99.99%, 1.5 cm^2). The PtAuP layer was then coated on the surface of ZnO to form ZnO@PtAuP alloy nanorod arrays (ANRAs) by co-electrodepositon in solution of 0.58×10^{-3} M $H_2PtCl_6{\cdot}6H_2O$ + 0.54×10^{-3} M $HAuCl_4{\cdot}3H_2O$ + 2.84×10^{-3} M $NaH_2PO_2{\cdot}H_2O$ + 0.34×10^{-3} M $C_6H_5Na_3O_7{\cdot}2H_2O$ (pH value was controlled to 3.5 by adding Na_2CO_3) at 0.25 mA cm^{-2} for 20 min at 50 °C. PtAuP alloy nanotube arrays were then obtained by immersing ZnO@PtAuP ANRAs in H_2SO_4 solution (pH value was 2.5) for 3 h to completely remove ZnO NRAs template. For the comparative study, PtAu ANTAs were also synthesized with the similar methods described above without $NaH_2PO_2{\cdot}H_2O$.

Materials Characterization: The structures of these catalysts were characterized by XRD (Bruker D8 Advance). The morphologies were examined by SEM (NOVA NANOSEM 430), TEM (JEM-2100F), and EDS (XFlash 5030T). Chemical-state analysis was carried out by XPS (ESCALAB 250). All XPS spectra were corrected using the C 1s line at 284.6 eV. Curve fitting and background subtraction were accomplished.

Electrode Preparation and Electrochemical Measurements: To compare the electrocatalytic properties of PtAuP ANTAs, PtAu ANTAs and commercial Pt/C, we loaded 2.248 μg PtAuP ANTAs, 2.118 μg PtAu ANTAs and 5 μg Pt/C on a glassy carbon electrode (GCE, d = 3 mm), respectively (Pt loading: ≈14 μg cm^{-2}). The commercial Pt/C ink (2 mg mL^{-1}) was prepared by mixing the catalyst with a 5 wt% Nafion ionomer solution in ethanol absolute under ultrasonication for 10 min, 2.5 μL Pt/C ink was then deposited

on the GCE. A small piece of as-prepared PtAuP ANTAs and PtAu ANTAs were adhered directly on the GCE using Nafion ionomer solution. Electrochemical measurements were performed with a CHI 604D electrochemical workstation. A standard three-electrode cell was used for all electrochemical experiments, which consisted of a Pt wire as the counter electrode, a saturated calomel electrode (SCE) as the reference electrode, and modified catalyst/GCE as the working electrode. CV was carried out in 0.5 M H_2SO_4 between –0.24 and 0.96 V (vs SCE) with a scan rate of 50 mV s^{-1}. For CV and chronoamperometry measurements of methanol oxidation reactions, an aqueous solution of 0.5 M CH_3OH + 0.5 M H_2SO_4 was utilized. And chronoamperometry curves were recorded at 0.60 V (vs SCE). The CO stripping measurements were finished in 0.5 M H_2SO_4. Before CO stripping, the electrode was immersed in a CO-saturated electrolyte at 0 V for 15 min. After that, the electrolyte was purged with pure N_2 and two consecutive CVs were then recorded (CO stripping and after stripping). All electrochemical measurements were carried out at room temperature, and all reported potentials were relative to the reversible hydrogen electrode (RHE).

Supporting Information

Supporting Information is available from the Wiley Online Library or from the author.

Acknowledgements

The authors acknowledge the support of the National Natural Science Foundation of China (21406078), National Key R&D Program (2016YFA0202601), the Pearl River and S&T Nova Program of Guangzhou (201610010076), and Fundamental Research Funds for the Central Universities.

[1] a) A. Arico, S. Srinivasan, V. Antonucci, *Fuel cells* **2001**, *1*, 133; b) Y. Paik, S. S. Kim, O. H. Han, *Angew. Chem. Int. Ed.* **2008**, *47*, 94; c) Z. M. Cui, M. H. Yang, F. J. DiSalvo, *ACS Nano* **2014**, *8*, 6106; d) Z. M. Cui, H. Chen, M. T. Zhao, D. Marshall, Y. C. Yu, H. Abruña, F. J. DiSalvo, *J. Am. Chem. Soc.* **2014**, *136*, 10206.

[2] a) N. Marković, P. N. Ross, *Surf. Sci. Rep.* **2002**, *45*, 117; b) T. Iwasita, *Electrochim. Acta* **2002**, *47*, 3663; c) F. Liu, J. Y. Lee, W. J. Zhou, *Small* **2006**, *2*, 121; d) F. Saleem, B. Ni, Y. Yong, L. Gu, X. Wang, *Small* **2016**, *12*, 5261.

[3] a) X. Huang, Y. Chen, E. Zhu, Y. Xu, X. Duan, Y. Huang, *J. Mater. Chem. A* **2013**, *1*, 14449; b) H. Zhang, M. Jin, Y. Xia, *Chem. Soc. Rev.* **2012**, *41*, 8035; c) M. Chen, B. Wu, J. Yang, N. Zheng, *Adv. Mater.* **2012**, *24*, 862.

[4] a) J.-H. Choi, K.-W. Park, I.-S. Park, K. Kim, J.-S. Lee, Y.-E. Sung, *J. Electrochem. Soc.* **2006**, *153*, A1812; b) C. Zhu, S. Guo, S. Dong, *Adv. Mater.* **2012**, *24*, 2326; c) C. Hu, H. Cheng, Y. Zhao, Y. Hu, Y. Liu, L. Dai, L. Qu, *Adv. Mater.* **2012**, *24*, 5493.

[5] a) V. Grozovski, V. Climent, E. Herrero, J. M. Feliu, *J. Electroanal. Chem.* **2011**, *662*, 43; b) Z. Liu, G. S. Jackson, B. W. Eichhorn, *Energy Environ. Sci.* **2011**, *4*, 1900; c) Y.-J. Deng, N. Tian, Z.-Y. Zhou, R. Huang, Z.-L. Liu, J. Xiao, S.-G. Sun, *Chem. Sci.* **2012**, *3*, 1157; d) K. Sasaki, H. Naohara, Y. Choi, Y. Cai, W.-F. Chen, P. Liu, R. R. Adzic, *Nat. Commun.* **2012**, *3*, 1115; e) R. Wang, C. Wang, W. B. Cai, Y. Ding, *Adv. Mater.* **2010**, *22*, 1845.

[6] a) L.-X. Ding, A.-L. Wang, G.-R. Li, Z.-Q. Liu, W.-X. Zhao, C.-Y. Su, Y.-X. Tong, *J. Am. Chem. Soc.* **2012**, *134*, 5730; b) H. You, F. Zhang, Z. Liu, J. Fang, *ACS Catal.* **2014**, *4*, 2829; c) L. Dai, S. G. Mo, Q. Qin, X. J. Zhao, N. F. Zheng, *Small* **2016**, *12*, 1572.

[7] a) S. Zhou, K. McIlwrath, G. Jackson, B. Eichhorn, *J. Am. Chem. Soc.* **2006**, *128*, 1780; b) M. Schrinner, S. Proch, Y. Mei, R. Kempe, N. Miyajima, M. Ballauff, *Adv. Mater.* **2008**, *20*, 1928; c) M. Chen, D. Goodman, *Science* **2004**, *306*, 252; d) S. Daniells, A. Overweg, M. Makkee, J. Moulijn, *J. Catal.* **2005**, *230*, 52; e) D. A. Bulushev, I. Yuranov, E. I. Suvorova, P. A. Buffat, L. Kiwi-Minsker, *J. Catal.* **2004**, *224*, 8.

[8] J. Zhang, K. Sasaki, E. Sutter, R. Adzic, *Science* **2007**, *315*, 220.

[9] S. Zhang, Y. Shao, H.-g. Liao, J. Liu, I. A. Aksay, G. Yin, Y. Lin, *Chem. Mater.* **2011**, *23*, 1079.

[10] a) K. Mikkelsen, B. Cassidy, N. Hofstetter, L. Bergquist, A. Taylor, D. A. Rider, *Chem. Mater.* **2014**, *26*, 6928; b) I.-S. Park, K.-S. Lee, J.-H. Choi, H.-Y. Park, Y.-E. Sung, *J. Phys. Chem. C* **2007**, *111*, 19126; c) J. Zhang, D. N. Oko, S. b. Garbarino, R. g. Imbeault, M. Chaker, A. C. Tavares, D. Guay, D. Ma, *J. Phys. Chem. C* **2012**, *116*, 13413; d) V. Petkov, B. N. Wanjala, R. Loukrakpam, J. Luo, L. Yang, C.-J. Zhong, S. Shastri, *Nano Lett.* **2012**, *12*, 4289; e) W. Hong, J. Wang, E. Wang, *Small* **2014**, *10*, 3262.

[11] a) S. Yan, S. Zhang, W. Zhang, J. Li, L. Gao, Y. Yang, Y. Gao, *J. Phys. Chem. C* **2014**, *118*, 29845; b) J. Zeng, J. Yang, J. Y. Lee, W. Zhou, *J. Phys. Chem. B* **2006**, *110*, 24606.

[12] Y. Kim, H. J. Kim, Y. S. Kim, S. M. Choi, M. H. Seo, W. B. Kim, *J. Phys. Chem. C* **2012**, *116*, 18093.

[13] a) P. Hernández-Fernández, S. Rojas, P. Ocon, J. Gómez de la Fuente, J. San Fabián, J. Sanza, M. Pena, F. García-García, P. Terreros, J. Fierro, *J. Phys. Chem. C* **2007**, *111*, 2913; b) Z. Peng, H. Yang, *Nano Res.* **2009**, *2*, 406.

[14] a) X. Sun, D. Li, Y. Ding, W. Zhu, S. Guo, Z. L. Wang, S. Sun, *J. Am. Chem. Soc.* **2014**, *136*, 5745; b) S. Zhang, S. Guo, H. Zhu, D. Su, S. Sun, *J. Am. Chem. Soc.* **2012**, *134*, 5060; c) C. Zhu, S. Guo, S. Dong, *J. Mater. Chem.* **2012**, *22*, 14851; d) J. Sun, H. Ma, H. Jiang, L. Dang, Q. Lu, F. Gao, *J. Mater. Chem. A* **2015**, *3*, 15882; e) A. Dutta, J. Ouyang, *ACS Catal.* **2015**, *5*, 1371; f) X. H. Tan, S. Prabhudev, A. Kohandehghan, D. Karpuzov, G. A. Botton, D. Mitlin, *ACS Catal.* **2015**, *5*, 1513.

[15] a) S. Park, Y. Xie, M. J. Weaver, *Langmuir* **2002**, *18*, 5792; b) D. Yuan, X. Gong, R. Wu, *J. Chem. Phys.* **2008**, *128*, 064706; c) Y. X. Chen, A. Miki, S. Ye, H. Sakai, M. Osawa, *J. Am. Chem. Soc.* **2003**, *125*, 3680; d) T. Yajima, H. Uchida, M. Watanabe, *J. Phys. Chem. B* **2004**, *108*, 2654.

[16] a) P. Ferrin, M. Mavrikakis, *J. Am. Chem. Soc.* **2009**, *131*, 14381; b) J.-H. Ma, Y.-Y. Feng, J. Yu, D. Zhao, A.-J. Wang, B.-Q. Xu, *J. Catal.* **2010**, *275*, 34.

[17] M. Yin, Y. Huang, L. Liang, J. Liao, C. Liu, W. Xing, *Chem. Commun.* **2011**, *47*, 8172.

[18] W. Zhong, Y. Liu, D. Zhang, *J. Phys. Chem. C* **2012**, *116*, 2994.

[19] a) K. C. Poon, D. C. Tan, T. D. Vo, B. Khezri, H. Su, R. D. Webster, H. Sato, *J. Am. Chem. Soc.* **2014**, *136*, 5217; b) Y. Hu, J. O. Jensen, W. Zhang, L. N. Cleemann, W. Xing, N. J. Bjerrum, Q. Li, *Angew. Chem. Int. Ed.* **2014**, *53*, 3675; c) G. Yang, Y. Chen, Y. Zhou, Y. Tang, T. Lu, *Electrochem. Commun.* **2010**, *12*, 492; d) J. Tian, Q. Liu, N. Cheng, A. M. Asiri, X. Sun, *Angew. Chem. Int. Ed.* **2014**, *53*, 9577; e) Q. Liu, J. Tian, W. Cui, P. Jiang, N. Cheng, A. M. Asiri, X. Sun, *Angew. Chem. Int. Ed.* **2014**, *126*, 6828; f) J. Chang, L. Feng, C. Liu, W. Xing, X. Hu, *Angew. Chem. Int. Ed.* **2014**, *53*, 122; g) X. Xue, J. Ge, C. Liu, W. Xing, T. Lu, *Electrochem. Commun.* **2006**, *8*, 1280; h) X. Xue, J. Ge, T. Tian, C. Liu, W. Xing, T. Lu, *J. Power Sources* **2007**, *172*, 560.

[20] a) L. Liu, E. Pippel, R. Scholz, U. Gösele, *Nano Lett.* **2009**, *9*, 4352; b) L. L. Zhang, M. Wei, S. Q. Wang, Z. Li, L.-X. Ding, H. H. Wang, *Chem. Sci.* **2015**, *6*, 3211.

[21] Z. Wen, Q. Wang, J. Li, *Adv. Funct. Mater.* **2008**, *18*, 959.
[22] J. N. Tiwari, F.-M. Pan, K.-L. Lin, *New J. Chem.* **2009**, *33*, 1482.
[23] a) P. Luksirikul, K. Tedsree, M. G. Moloney, M. L. H. Green, S. C. E. Tsang, *Angew. Chem. Int. Ed.* **2012**, *51*, 6998; b) G. X. Chen, C. F. Xu, X. Q. Huang, J. Y. Ye, L. Gu, G. Li, Z. C. Tang, B. H. Wu, H. Y. Yang, Z. P. Zhao, Z. Y. Zhou, G. Fu, N. F. Zheng, *Nat. Mater.* **2016**, *15*, 564.
[24] J. F. C, L. G. Feng, C. P. Liu, W. Xing, X. L. Hu, *Energy Environ. Sci.* **2014**, *7*, 1628.
[25] a) Z. M. Cui, C. X. Guo, C. M. Li, *J. Mater. Chem. A* **2013**, *1*, 6687; b) J. F. Xu, X. Y. Liu, Y. Chen, Y. M. Zhou, T. H. Lu, Y. W. Tang, *J. Mater. Chem.* **2012**, *22*, 23659; c) M. X. Gong, G. T. Fu, Y. Chen, Y. W. Tang, T. H. Lu, *ACS Appl. Mater. Inter.* **2014**, *6*, 7301.

Received: November 30, 2016
Revised: January 20, 2017
Published online:

